

Potential-Dependent Pt(111)/Water Interface: Tackling the Challenge of a Consistent Treatment of Electrochemical Interfaces**

Laura Braunwarth⁺,^[a] Christoph Jung⁺,^{*[a, b, c]} and Timo Jacob^{*[a, b, c]}

The interface between an electrode and an electrolyte is where electrochemical processes take place for countless technologically important applications. Despite its high relevance and intense efforts to elucidate it, a description of the interfacial structure and, in particular, the dynamics of the electric double layer at the atomic level is still lacking. Here we present reactive force-field molecular dynamics simulations of electrified Pt(111)/water interfaces, shedding light on the orientation of water molecules in the vicinity of the Pt(111) surface, taking into account the influence of potential, adsorbates, and ions simultaneously. We obtain a shift in the preferred orientation of

water in the surface oxidation potential region, which breaks with the previously proclaimed strict correlation to the free charge density. Moreover, the characterization is complemented by course of the entropy and the intermolecular ordering in the interfacial region complements the characterization. Our work contributes to the ongoing process of understanding electric double layers and, in particular, the structure of the electrified Pt(111)/water interface, and aims to provide insights into the electrochemical processes occurring there.

Introduction

At the interface between an electrode and an electrolyte, the electric double layer (EDL) is formed, which is characterized by a considerable potential change within a few Angströms and a complex interplay of charges between solvent dipoles, charged adsorbates, and the diffuse ion layer. A deeper understanding of EDL is a compelling need for knowledge-based progress in electrochemical processes occurring in technologically relevant areas such as energy conversion, storage devices and solar cells.^[1–4] Despite their great importance, a complete and comprehensive description of EDL at the atomic level, including interfacial structures and dynamics, has been lacking. The

complexity and difficulty of studying them have been addressed in recent years both experimentally (e.g. using X-ray photoelectron spectroscopy (XPS),^[1] Raman spectroscopy,^[5,6] laser-induced temperature jump methods,^[7] Cyclic voltammetry (CV)^[8] or sum frequency generation spectroscopy^[9]) and theoretically via empirical interatomic force field simulations and first-principles calculations (e.g. *ab initio* molecular dynamics (AIMD),^[10,11] see also Ref. [12, 13] and references therein).

Although theoretical approaches are attractive because they can provide structural information and insight into the dynamic processes of electrified interfaces at the atomistic level and complement experiments, several challenges remain to be overcome. Several strategies have been developed to incorporate electrode potential into simulations, such as the widely employed computational standard hydrogen electrode scheme,^[14] in which the metal electrode exchanges electrons with a reservoir,^[15] constant Fermi level molecular dynamics,^[16,17] the electronegativity offset method,^[18] by introducing fixed excess charges^[10,19] or homogeneous background charges.^[20] The description of the aqueous electrolyte also differs: From implicit treatment of the solvent as a dielectric medium,^[21,22] to explicit but static solvent molecules localized at the electrode,^[23,24] to fully explicit modeling of the electrolyte.^[10,11] Although explicit modeling is advantageous in terms of polarization, solvation, and accuracy, the higher computational costs must be considered (e.g. limiting the number of solvent molecules in AIMD simulations to about 100). Here, force field methods can complement first-principles calculations by covering much larger time and length scales while still providing atomistic, mechanistic, and dynamical information. Even the early conception of a frozen bilayer structure of interfacial water on certain transition metal surfaces was modified by the inclusion of some degree of disorder, underscoring the

[a] Dr. L. Braunwarth,⁺ Dr. C. Jung,⁺ Prof. Dr. T. Jacob
Institute of Electrochemistry, Ulm University, Albert-Einstein-Allee 47, D-89081 Ulm, Germany


[b] Dr. C. Jung,⁺ Prof. Dr. T. Jacob
Karlsruhe Institute of Technology (KIT), P.O. Box 3640, D-76021 Karlsruhe, Germany
E-mail: christoph.jung@kit.edu
timo.jacob@uni-ulm.de

[c] Dr. C. Jung,⁺ Prof. Dr. T. Jacob
Helmholtz Institute Ulm (HIU) Electrochemical Energy Storage, Helmholtzstr. 11, D-89081 Ulm, Germany

[⁺] These authors contributed equally.

[**] A previous version of this manuscript has been deposited on a preprint server (DOI: <https://chemrxiv.org/engage/chemrxiv/article-details/625579e7ef2ade874b2ca57c>)

 Supporting information for this article is available on the WWW under <https://doi.org/10.1002/cphc.202200336>

 © 2022 The Authors. ChemPhysChem published by Wiley-VCH GmbH. This is an open access article under the terms of the Creative Commons Attribution Non-Commercial NoDerivs License, which permits use and distribution in any medium, provided the original work is properly cited, the use is non-commercial and no modifications or adaptations are made.

importance of including water dynamics.^[25–30] Although adsorbates affect the properties of the solvation layer, they have not been included in the interface system in most AIMD simulations, with the exception of selected studies that consider adsorbed hydrogen^[31–33] or hydroxide.^[30] However, adsorbates are of particular interest in simulating the platinum/water interface: More detailed insights into the effects of surface coverage on the interfacial structure of the adsorbed water layer are urgently needed, taking into account the coverage of the electrode with oxygen-containing intermediates at electrode potentials relevant to catalytic reactions (e.g. oxygen reduction reaction).

Recently, Le *et al.* have performed state-of-the-art AIMD simulations to investigate the relationship between the molecular structure of the Pt(111)/water interface and its capacitive behavior.^[10] Sakong *et al.* have studied the mobility and orientation of the water molecules in the adsorbate layer on the same surface, including the variation of the potential.^[11] Bouzid *et al.* also studied the structural reorganization of the electrical double layer as a function of the potential with Fermi level molecular dynamics and observed a so-called flip-flop behavior: The dipole of the water molecule points toward (or away) from the Pt(111) surface when negatively (or positively) charged.^[17] However, the question of how water behaves at the interface when all relevant factors (e.g. potential, adsorbates, and ions) are considered simultaneously remains unanswered.

Motivated by these questions, in the present work we have performed extensive ReaxFF studies on the reactive molecular dynamics (MD) of the Pt(111)/water interface, including the influence of an electrode potential as a function of surface charge densities and surface coverages of oxygen-containing intermediates. In contrast to several previous studies, we provide a fully self-consistent description of the entire electrochemical interface, including both the surface and an extended portion of the electrolyte region. We present a detailed analysis of the variation of the water orientation at the interface as a function of the applied potential. Our calculations show that the H-down orientation, where an O–H bond is directed toward the surface, is preferred in the region of the surface oxidation potential region. We further elucidate the thermodynamics of the Pt(111)/water interface by evaluating the progression of entropy from the bulk water to the adsorbed water layer. Our work demonstrates the importance of adding to the picture of the potential-dependent structure and dynamics of the EDL at the molecular level.

Methods

ReaxFF

The ReaxFF reactive force field method is based on a bond order-dependent potential energy term combined with a time-dependent polarizable charge description.^[34,35] Bonding terms (e.g. bond, angle and torsion contributions; inherently depending on the bond order) and non-bonding interaction terms (e.g. van der Waals, Coulomb interactions and hydrogen bonds)

contribute to the potential energy formulation. The bond order is updated at each iteration step, controlled by the local atomic environment. In this way, both bond formation and dissociation can be captured. The self-consistent electron equilibration method (EEM) by Mortier *et al.*^[36] is used to determine the partial charges of each atom and to describe electrostatic interactions. Our self-developed Pt/O/H reactive force field by D. Fantauzzi *et al.*^[37] serves as the atomistic potential for the platinum, the oxygen-containing intermediates, and water, extended by the reactive force field parameters for K⁺ and F[−] ions.^[38] There, the interactions between the electrolyte ions and water were extensively validated, while in our previous work (Ref. [37]), the force field for platinum bulk and surfaces including the surface oxide formation of the Pt(111) surface was intensively tested. Note that no direct bonding terms are considered between the charged ions and the surface, as these ions are assumed to keep their solvation shell. However, all elements (including the ions) were considered in all non-bonded interactions. All ReaxFF calculations were performed using the ADF software package (version 2019.103).^[39,40] In general, a time step of 0.25 fs was used to integrate the equations of motion using the Velocity-Verlet algorithm. This short time step is sufficient to properly describe the smallest oscillations in the system, which are the hydrogen stretching oscillations. The Nosé–Hoover thermostat with a damping constant of 100 fs set the temperature for the MD simulations to 298.15 K.^[41,42] Regarding the thermostat, for selected model systems we compared the Nosé–Hoover as well as the Berendsen thermostats (both available in the ADF package suite), showing a consistent behavior. The Pt(111) surface was modeled by a symmetric twelve-layer slab (10 × 10 × 12 atoms) with the two middle layers fixed to the corresponding calculated bulk crystal structure. For convergence studies of the platinum crystal distance, the number of layers, and the size of the unit cell, we refer to the paper by Fantauzzi *et al.* (Ref. 37) Normal to the surface planes, the Pt slab is in contact with a 50 Å thick water layer ($\rho = 0.997 \text{ g/cm}^3$), e.g. 2306 water molecules. The selected size of the water box is based on the findings published in Ref. 43. The systems were created using packmol software.^[44] All systems presented here were equilibrated for 400,000 iterations in the canonical NVT ensemble, followed by a production run for an additional 400,000 iterations. Two-phase thermodynamics (2PT) calculations were performed to evaluate the spatially resolved entropy of water layers, with the NVT run followed by 50,000 iterations in the microcanonical NVE ensemble plus 5,000 iterations for evaluation within the 2PT method. For a detailed description of the method as well as the coupling between the 2PT method (developed by Lin *et al.*^[45,46]) and ReaxFF, we refer the reader to our recent publication.^[43] Structure visualizations were performed using VMD software.^[47]

Introducing the Electrode Potential in ReaxFF MD Simulations

Double Layer Potential Region

The electrified Pt(111)/H₂O interfaces were made by placing charges on the platinum slab, thus assuming thereby premising the established conception of the free charge density being a good approximation of the electrode potential.^[6,10,48] Here, Gauthier *et al.* also consider the effective free charge density as a descriptor for the electrochemical driving force of processes, which is preferable to the work function approach because of its sensitivity to the size of the simulation cells.^[48] The free charge density (denoted $\sigma_{\text{Pt}_{\text{IL}}}$) here describes the actual charge located on the electrode side of the EDL, compensated by the ionic charge in the electrolyte in the absence of specific adsorption of hydrogen or hydroxide.^[7,49,50] The free charge density curves obtained by Garcia *et al.* using the laser-induced temperature jump method for the Pt(111) surface in 0.1 M HClO₄ serve as a reference for introducing the electrode potential into our simulations.^[7] Note that via experimental cyclic voltammetric measurements, the total charge density is accessible, including the charge transferred during adsorption processes (e.g. when chemical bonds are formed). In the following interfacial characterization under double layer potential conditions ($E \leq 0.5$ V), we assume an adsorbate-free surface, therefore the equality of free charge density and total charge density holds true.

For our simulations, a series of electrified Pt(111)/water interface models with different free charge densities were created; for the charge neutrality of the double layer, $\sigma_{\text{Pt}_{\text{IL}}}$ is compensated by counterions. A detailed explanation of the methodological setup can be found in the Supporting Information (SI), where the nature of the charges as well as their location and the counterions present are also described. Furthermore, due to the charge balance equilibration approach in ReaxFF, the atomic charges of platinum are not fixed, but

allowed to fluctuate (dynamically determined by the local environment), with the only constraint being the given total charge of the slab. The resulting charge on the atoms of the surface layer gives a specific surface charge density corresponding to a certain electrode potential (see Figure S2 of the SI). Depending on the electrode potential, the charge distribution within the platinum slab differs, though showing some common features: As shown in Figure 1 (b), the main charge is located in the surface layers of the symmetric platinum slab (labelled Pt_{1L}). Subsequent layers show a slight Friedel oscillation until the atomic charges deviate only slightly from the mean bulk charge.^[33] To account for charge compensation of the platinum surface, counterions, *i.e.* K⁺ and F⁻, are introduced into the system and are located both in the outer Helmholtz plane and in the subsequent diffuse layer, see Figure 1 (a).

This approach provides a self-consistent description of the entire electrochemical interface and thus promises a more realistic ion distribution compared to homogeneous background charges, the use of an effective screening medium, or Gaussian charge sheets commonly used in AIMD simulations.^[17,20,51–53] Because ReaxFF allows nanosecond-scale simulations, the interface, including the ion distribution, is sufficiently equilibrated, which also allows extensive and representative sampling of the phase-space.^[51]

The $\sigma_{\text{Pt}_{\text{IL}}}$ (see Figure S2 of the SI) shows good agreement with the surface charge density obtained using the laser-pulsed jump technique by Garcia *et al.*^[7] The location of the zero crossing at about 0.3 V, which corresponds to the point of zero free charge and is in good accordance. Following the evolution of the double-layer charge as a function of the simulated electrode potential, the hump-shaped, bell-shaped course of the double-layer capacitance C_{dl} is obtained, as shown in SI Figure S2. Here, the peak around 0.3 V describes a significant change in the double-layer capacitance, presumably caused by structural rearrangements of the EDL.^[10,54] In particular, a potential-dependent adsorption/desorption behavior of H₂O or

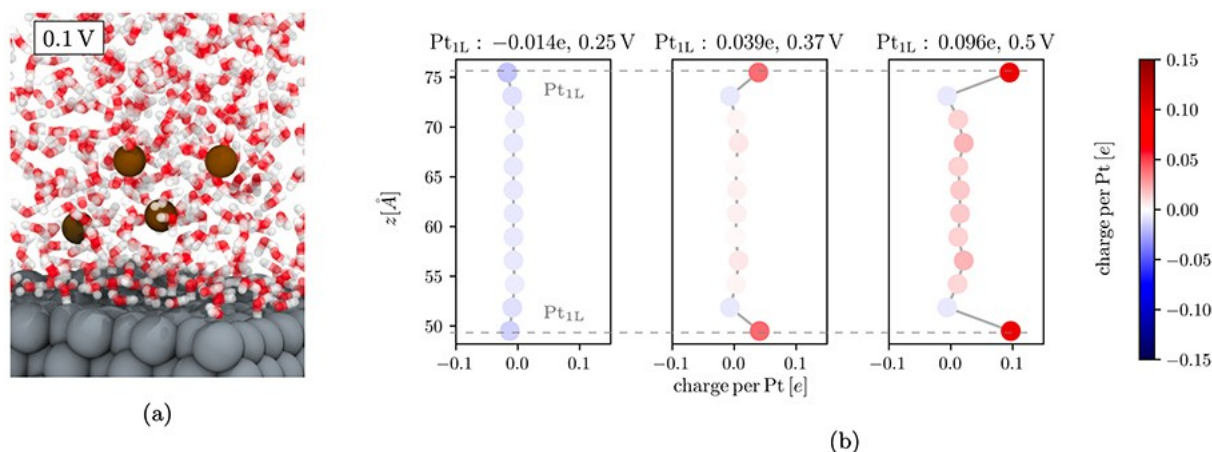


Figure 1. (a) Representative snapshot of the Pt(111)/H₂O interface at a potential corresponding to 0.1 V vs. SHE. The Pt and K⁺ atoms are colored in gray and brown, the water molecules are shown as red and white sticks for sake of clarity. (b) For the atomic charge distribution in the individual layers of the Pt slab, the mean atomic charge per layer is color coded between red (partially positive) and blue (partially negative). The topmost and lowest balls correspond to the surface layers (denoted: Pt_{1L}).

its orientational ordering in the interface could be important here. In the following, we investigate these properties self-consistently in detail.

Surface Oxidation Potential Region

In the double layer potential region, we could relate the charge density of the adsorbate-free Pt(111) surface to the electrode potential. However, the transition to higher potentials requires consideration of appropriate adsorbate compositions (*i.e.*, oxygen atoms O*, hydroxide molecules OH*, and water molecules H₂O*) and surface oxidation effects. In the following, we formulate and apply a structure–potential–relation connecting a given electrode potential to the corresponding equilibrium surface structure as predicted in the literature. In this sense, the theoretical studies by Kronberg *et al.*^[31] and Sakong *et al.*^[33] have recently included hydrogenated Pt(111) surfaces to approximate the low potential region. To date, the authors are not aware of any similar approaches for modeling the higher potential region that consistently include all relevant oxygen-containing adsorbates.

As can be seen from experimental observations (e.g. XPS,^[1,55,56] CV^[57]) and theoretical predictions,^[58] OH* appears on the Pt(111) surface due to H₂O oxidation from about 0.6 V onward. This coverage becomes dominant around 0.8 V, while less H₂O* is adsorbed on the surface. As the potential increases, O* occurs by oxidation of OH* and becomes the dominant surface species at potentials near 1 V.

In Figure 2 (a), the realization of the potential-dependent surface coverages in our simulations are displayed. The depicted composition of oxygenated adsorbates is thermodynamically stable and mirrors the corresponding electrochemical environment at the respective electrode potential, without including the potential as an explicit parameter of the simulation. The total coverage of OH*, H₂O* and O* is around 0.6 ML over the whole potential range. This resembles the coverage as known from traditional water bilayer models,

demanding an intensive structural elucidation of the hydrogen bonding present and adsorbate configurations (see results section). For a description of the location of charges and the total amount of K⁺ and F[−] ions, see the SI.

For verifying our structure–potential–relation the structural model of the electrified Pt(111) interface by Huang *et al.* serves as benchmark.^[59] Within their model, the authors include parameter-based submodels for an oxide layer, the water layer and the diffuse layer. They are consequently able to deconvolute the total charge density into contributions arising from Pt oxidation (σ_{ox}) or hydrogen adsorption and the free surface charge density σ_M . σ_M itself is associated to the dipole moment of the oxide layer, the water dipole in the interfacial electric field and the pure double-layer charging. In our simulations, the deconvolution is not required as the interface is treated self-consistently. We calculate σ_M as the charge density of the Pt surface layer including the partial charges of oxygenated intermediates and adsorbed H₂O* molecules. Correlating the respective surface coverages of OH*, H₂O* and O* to the expected number of transferred electrons upon adsorption, σ_{ox} is obtained. Here, we can reproduce the course of σ_M in the structural model by Huang *et al.* along with the location of zero-crossing, as well as the magnitude of the charge density in the potential range between 0.65 and 1.0 V, see Figure 2 (b).

We have presented two approaches to include the effects of an electrode potential into ReaxFF simulations: First, the double layer potential region (up to 0.5 V) is installed over the potential-defining free charge densities on the adsorbate-free Pt(111) surface. Second, in the surface oxidation potential region (0.65–1.0 V) the stable coverages of oxygenated intermediates on the Pt(111) surface define the free surface charge density and correlate to a specific electrode potential.

Results and Discussion

The orientation of the interfacial water molecules is influenced by the chemical interactions between platinum and water, the

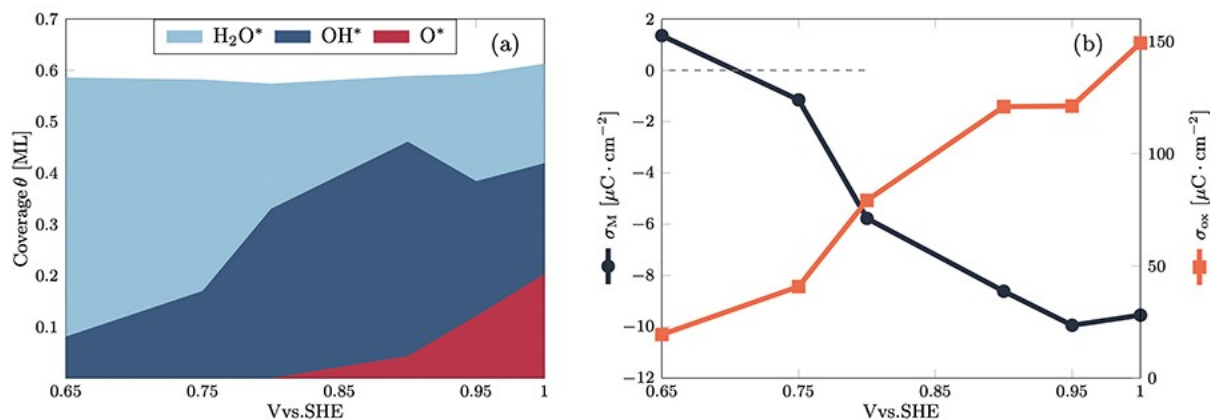


Figure 2. (a) The potential-dependent surface coverages of H₂O*, OH* and O* are displayed as stacked area chart. The total surface coverage is observed to be around 0.6 ML throughout this potential region here. (b) The free charge density at the Platinum surface σ_M in dark blue and the charge density transferred in surface oxidation σ_{ox} in orange are displayed.

free charge density (affecting the direction of the water dipoles) as well as the presence of adsorbates (through blocking of sites and manipulating the electrostatic effect of the free charge density). Here, three main configurations of interfacial water can be distinguished: H₂O-parallel, with the molecule adsorbed via the oxygen atom on a top-site of the Pt surface and both hydrogen atoms slightly tilted away from the surface. H-up, where one hydrogen atom points away from the surface and H-down with one hydrogen atom directed towards the surface, see Figure 3 for visualization. Numerous studies have contributed here, obtaining small to negligible differences in stability between the two orientations.^[25,27,60–63] In the following, we focus on – with no claim to completeness – experimental and theoretical work including the electrode potential into their investigation of the Pt/H₂O interface. In our ReaxFF-MD study, we observe a change of the preferred orientation of interfacial H₂O from H-up to H-down with increasing electrode potential. To the author's knowledge, this shift to a dominating H-down configuration in the surface oxidation potential region is so far undocumented. A detailed discussion of the structure of the water layer as well as the occurrence of ordered patterns will be presented together with the spatially-resolved entropy behavior later. Near the assumed location of the potential of zero charge (*pzc*, ~0.3 V), both H-up and H-down orientations of the interfacial water molecules (e.g. H₂O within 3.5 Å distance to the Pt surface) are observed. In Figure 3, this is represented by a comparable proportion of both configurations. Up to 0.5 V, the H-up orientation is distinctly preferred, in line with AIMD studies.^[10,11,31] This indicates a strong correlation between the water orientation and the free charge density, as with a more positively charged surface the hydrogen atoms tend to point away from the surface.

Also, the surface coverage of H₂O* is increasing in this potential region, up to 0.76 ML at 0.5 V. Following Le *et al.*'s argumentation, this increase in coverage induces a significant interface dipole potential change and causes a negative capacitance.^[10] This is in line with the obtained one-humped

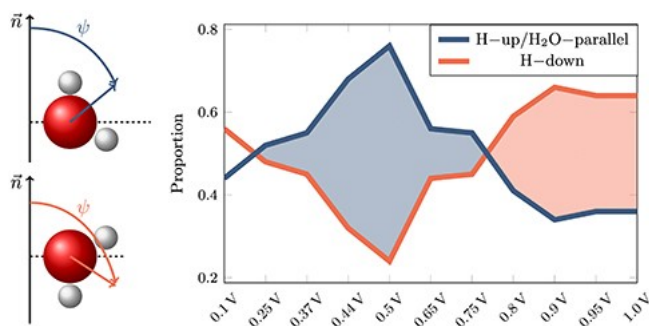


Figure 3. Depending on the applied electrode potential, the orientation of the adsorbed water molecules on the Pt(111) surface is categorized as H-down or H-up/H₂O-parallel. Hereby, H-down corresponds to one hydrogen atom pointing towards the surface characterized by an angle $\psi > 90^\circ$ between the surface normal vector \vec{n} and the water bisector vector. Analogously, H-up corresponds to one hydrogen atom pointing away from the Pt surface and an angle $\psi < 90^\circ$. Shaded areas in the plot correspond to the dominating configuration in the respective potential region.

course of the differential double layer capacitance with its maximum near the *pzc* as depicted in Figure S2 of the SI. Singular occurrences of H₂O* dissociation, leading to H* and OH* can be detected. However, as soon as oxygenated intermediates are present on the Pt(111) surface, the proportion of H-down oriented H₂O* is increasing and from 0.8 V onwards dominating. The presence of negatively charged adsorbates (e.g. OH* and O*) promotes the reorientation of interfacial water molecules to pointing their positive charges on the hydrogen atoms towards the surface. This is visualized in Figure 3, where the H-down configuration is observed for up to 66% of the interfacial water molecules between 0.9 V and 1.0 V. The median of the angle ψ between the water bisector vector and the surface supports additionally our observation of the preference of the H-down configuration with increasing potential: ψ_{median} is changing from 61.7° at 0.44 V to its maximum value of 105.2° at 1.0 V. This reorientation is however restricted to the water molecules within a few Ångströms distance to the Pt(111) surface. Further away from the platinum surface, the water molecules shows random orientations and are only locally affected by charged ions. For a detailed study of the ion–water interaction the reader is referred to Ref. 38. As the orientation of the interfacial water molecules is a result of several (competing) influences, we expect the intermolecular ordering and hydrogen bonded network to be affected as well. For elucidation thereof, we investigated the course of the water's entropy at the Pt(111) interface in combination with the distribution profiles of water regarding the Pt–H₂O distance and the H₂O*–H₂O* in-plane distances.

We have successfully transferred the Two Phase Thermodynamics method (2PT) to the ReaxFF framework and the Pt(111)/H₂O interface for a structural and thermodynamical characterization thereof, see Ref. 43. This method constitutes the calculation of thermodynamical quantities by merely post-processing a molecular dynamics trajectory, dividing the density of states function of the liquid into a superposition of solid and diffusive contributions and thereon applying the respective thermodynamic theories. There, we have observed a significant reduction of the entropy *S* by nearly 50% in the adsorbed water layer on the Pt(111) surface at conditions of potential of zero charge compared to the entropy in bulk water. The bulk water entropy has been determined as $S_{\text{H}_2\text{O, bulk}} = 59.27 \text{ J/molK}$, deviating by 15% from the experimental value of $S_{\text{H}_2\text{O, exp}} = 69.95 \text{ J/molK}$.^[65] This underestimation occurs over several empirical water models, the main reason being too stiff hydrogen bonding interactions, and has been discussed in detail in our recent work.^[43] In Figure 4 (a), the potential-dependent evolution of the entropy from the adsorbed water layer into the bulk water is depicted. For the double layer potential region in general and exemplary at $E = 0.37 \text{ V}$, the reduced entropy of $S_{\text{H}_2\text{O}^*, 0.37 \text{ V}} = 29.57 \text{ J/molK}$ (compared to the bulk water entropy of $S_{\text{H}_2\text{O, bulk}} = 59.27 \text{ J/molK}$) suggests a higher ordering in the H₂O* adsorbate layer. This can be structurally resolved to the occurrence of (disordered patterns of) five-, six-, or seven-membered rings. However, due to the dynamics and thermal fluctuations, no ideal hexagonal hydrogen-bonded network can be observed. The effect of the charged platinum electrode onto

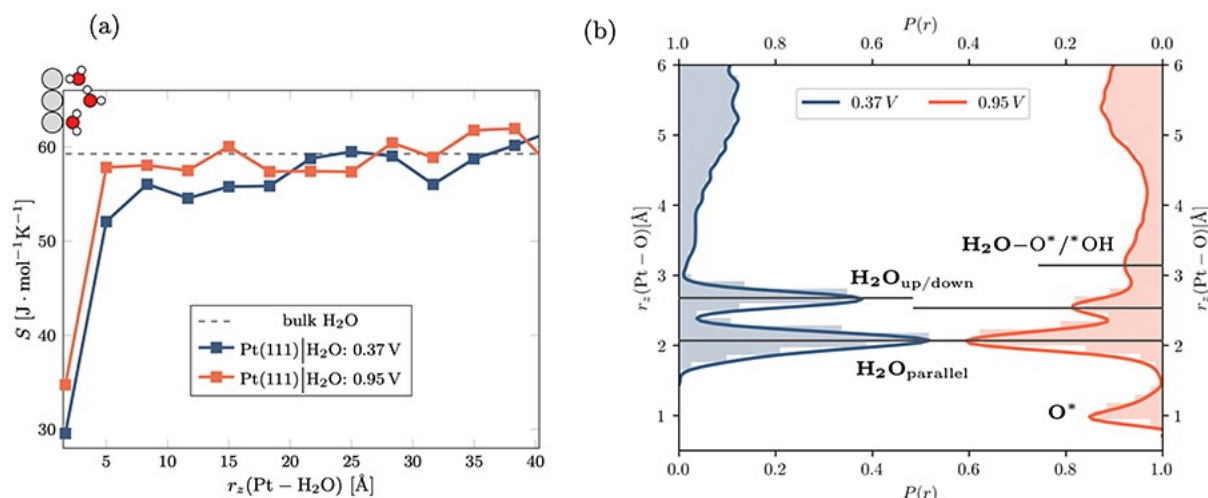


Figure 4. Variations on the electrode potential affect the thermodynamics of the Pt/ H_2O interface. In (a), the course of the entropy S for two simulated electrode potentials with increasing distance from the Pt(111) surface is depicted. Each data point has been calculated in a water layer of $\Delta z = 3.3 \text{ \AA}$. The dashed line represents the average H_2O bulk value of the entropy, 59.27 J/molK .^[43] (b) Oxygen distribution in z direction with increasing distance from the Pt surface for 0.37 V and 0.95 V electrode potential. Characteristic Pt– H_2O distances are labelled for comparison.

the water's entropy lasts up to a distance of 15–20 \AA , then the entropy fluctuates around the bulk value of $S_{\text{H}_2\text{O}, \text{bulk}}$. This observation is however dependent on the potential: From 0.1–0.5 V, the entropy reducing range of the Pt surface is increasing. The simultaneously growing proportion of H-up configurations of H_2O^* enables the formation of hydrogen bonds between the layer of adsorbed water molecules and the subsequent wetting layers. In contrast, under surface oxidation potential conditions the water's entropy regains its bulk value directly after the layer of adsorbed water ($S_{\text{H}_2\text{O}^*, 0.95 \text{ V}} = 34.73 \text{ J/molK}$). Here, the dominating H-down configuration induces hydrophobicity, as hydrogen bonding within the H_2O^* layer is encouraged while less hydrogen bonds are donated to the surrounding bulk water.^[65]

This can be also interpreted from Figure 4 (b) where the oxygen distribution with increasing distance to the Pt(111) surface is shown. While in the double layer potential region ($E \leq 0.5 \text{ V}$) only H_2O^* is present at the surface, producing two distinctive peaks of 2.1 \AA and 2.65 \AA , the distribution profile differs in the surface oxidation potential region ($E = 0.65\text{--}1.0 \text{ V}$): Here, additional peaks for O^* at 1.05 \AA and for H_2O molecules hydrogen bonded to O^* or OH^* at $\sim 3.1 \text{ \AA}$ appear. Depending on the respective local environment, the H-up or H-down configurations are located a bit closer to the Pt(111) surface. Subsequently at around 3–4 \AA , a nearly depleted region (e.g. low density area) contains mainly dangling hydrogen bonds. The width of this depleted region is again influenced by the applied electrode potential, spanning 1.6 \AA at 0.1 V to only 0.8 \AA at 0.5 V. Here, a balanced H-up/H-down proportion enables the formation of an intact intra- (e.g. within the adsorbed water layer) and interlayer (e.g. bridging the depleted region) hydrogen bond network (typical hydrogen bond length: 1.8 \AA). Meanwhile, an increasing occurrence of $\text{H}_2\text{O}_{\text{parallel}}$ or H-up configurations comprises the network and reduces the extent of layering in z direction. In the surface oxidation potential

region, due to the presence of oxygenated intermediates, the water layer is less homogeneous reflected by a less prominent adjacent depleted region and a more disconnected hydrogen bond network.

Lastly, to further elucidate the correlation between the entropy and structural ordering of water molecules on the Pt(111) surface, the $\text{H}_2\text{O}^* - \text{H}_2\text{O}^*$ distance distribution is evaluated. Here, the occurring distances are compared to the discrete distances of an ideal hexagonal water network, see Figure S3 in the SI, as well as Figures S4 and S5. In the double layer potential region, a distinct in-plane ordering of the adsorbed water molecules can be observed. With increasing potential though, a broadening of the peaks introduces noise, suggesting a less distinct ordering. This can be also traced back to the increasing coverage of H_2O^* , surpassing the coverage of the ideal hexagonal adsorbate structure (2/3 ML) at 0.37 V. For the surface oxidation potential region, the presence of O^* is deciding: For $E < 0.9 \text{ V}$, only OH^* and H_2O^* are present on the surface, which are maintaining a fairly ordered hydrogen bonded network, represented by discrete peaks in the O–O distance distribution. The presence of O^* however seriously disturbs the ordering on the surface and causes a broadening of the O–O distance distribution. In the water layer beyond the depleted region, in a distance of $\sim 4\text{--}6.5 \text{ \AA}$ to the Pt(111) surface, no ordering can be observed (independent of the applied potential). This is interpreted from a smooth distribution of the O–O distance distribution in Figure S3 (right) of the SI, featuring no distinct peaks as known from hexagonal motifs.

Conclusion

In the present work we present a self-consistent approach to handle the electrode potential in electrochemical interfaces,

based on the bond-order dependent ReaxFF force field molecular dynamics approach. This method was applied to describe the electrochemical interface between a Pt(111) electrode and different aqueous electrolytes, with a particular focus on the structure and properties of the predominant water within the interface region as function of the electrode potential. Here, the potential within the double layer region ($E < 0.5$ V) is reproduced by imposing a charge on the platinum slab, mirroring the free charge density on the surface as known from experimental studies. For the surface oxidation potential region ($E = 0.65$ – 1.0 V), the compositions of oxygenated intermediates on the Pt(111) surface (e.g. O^* , OH^* , H_2O^*) as known from literature are adapted and kept during the simulations, thereby premising a structure–potential–relation. Subsequently, the potential-dependent orientation of interfacial water is investigated, obtaining a shift of preference to H-down oriented adsorbed water in the surface oxidation potential region, due to the presence of oxygenated adsorbates. For investigation of the intermolecular water ordering and the hydrogen bonded network, the spatially resolved entropy of the water layers is calculated via the Two Phase Thermodynamics approach, which we have recently adapted to the ReaxFF force field framework.^[43] An enhanced ordering effect can be observed in the double layer potential region, where a balanced proportion of H-up and H-down configuration proves beneficial. Furthermore, our studies shed light on the interplay between water as electrolyte and the Pt(111) electrode, including the electrode potential, adsorbates and ions contributing to its still ongoing characterization and understanding process. As our approach realizes a self-consistent treatment of the electrochemical interface, our work demonstrates the capabilities of the ReaxFF method for the further clarification of the interface between electrode and electrolyte as well as the further optimization of electrochemical processes in heterogeneous catalysis.

Acknowledgement

This research was conducted as part of the German Research Foundation (DFG) under Project ID 390874152 (POLiS Cluster of Excellence) as well as the Sonderforschungsbereiche (collaborative research centers) SFB-1316 and SFB-1249. In addition, support from the BMBF (Bundesministerium für Bildung und Forschung) through the project InnoSüd (Grant Agreement: 03IHS024D) is gratefully acknowledged. Further, the authors acknowledge the computer time supported by the state of Baden-Württemberg through the bwHPC project and the DFG through grant number INST40/ 467–1 FUGG. The authors express their thanks to Andrey Sinyavskiy for coupling the 2PT method with ReaxFF and to Dr. Ludwig Kibler for fruitful discussions, sharing his impressive knowledge and asking the right questions. Open Access funding enabled and organized by Projekt DEAL.

Conflict of Interest

The authors declare no conflict of interest.

Data Availability Statement

The data that support the findings of this study are available in the supplementary material of this article.

Keywords: Electrochemical Interface · Force Field Simulations · Modeling · Platinum · Water

- [1] H. S. Casalongue, S. Kaya, V. Viswanathan, D. J. Miller, D. Friebel, H. A. Hansen, J. K. Nørskov, A. Nilsson, H. Ogasawara, *Nat. Commun.* **2013**, *4*, 2817.
- [2] I. Ledezma-Yanez, W. D. Z. Wallace, P. Sebastián-Pascual, V. Climent, J. M. Feliu, M. T. M. Koper, *Nat. Energy* **2017**, *2*, 17031.
- [3] F. Bella, C. Gerbaldi, C. Barolo, M. Grätzel, *Chem. Soc. Rev.* **2015**, *44*, 3431.
- [4] S. Xu, E. A. Carter, *Chem. Rev.* **2019**, *119*, 6631.
- [5] H. Shi, N. Poudel, B. Hou, L. Shen, J. Chen, A. V. Benderskii, S. B. Cronin, *Nanoscale* **2018**, *10*, 2398.
- [6] C.-Y. Li, J.-B. Le, Y.-H. Wang, S. Chen, Z.-L. Yang, J.-F. Li, J. Cheng, Z.-Q. Tian, *Nat. Mater.* **2019**, *18*, 697.
- [7] N. Garcia-Araez, V. Climent, J. Feliu, *J. Phys. Chem. C* **2009**, *113*, 9290.
- [8] K. Ojha, N. Arulmozhi, D. Aranzales, M. T. M. Koper, *Angew. Chem. Int. Ed.* **2020**, *59*, 711.
- [9] Z. D. Schultz, S. K. Shaw, A. A. Gewirth, *J. Am. Chem. Soc.* **2005**, *127*, 15916.
- [10] J.-B. Le, Q.-Y. Fan, J.-Q. Li, J. Cheng, *Sci. Adv.* **2020**, *6*.
- [11] S. Sakong, A. Groß, *Phys. Chem. Chem. Phys.* **2020**, *22*, 10431.
- [12] O. M. Magnussen, A. Groß, *J. Am. Chem. Soc.* **2019**, *141*, 4777.
- [13] O. Bjornholm, M. H. Hansen, A. Hodgson, L.-M. Liu, D. T. Limmer, A. Michaelides, P. Pedevilla, J. Rossmeisl, H. Shen, G. Tocci, E. Tyrode, M.-M. Walz, J. Werner, H. Bluhm, *Chem. Rev.* **2016**, *116*, 7698.
- [14] J. K. Nørskov, J. Rossmeisl, A. Logadottir, L. Lindqvist, J. R. Kitchin, T. Bligaard, H. Jónsson, *J. Phys. Chem. B* **2004**, *108*, 17886.
- [15] A. Y. Lozovoi, A. Alavi, J. Kohanoff, R. M. Lynden-Bell, *J. Chem. Phys.* **2001**, *115*, 1661.
- [16] A. Bouzid, A. Pasquarello, *J. Phys. Chem. Lett.* **2018**, *9*, 1880.
- [17] A. Bouzid, P. Gono, A. Pasquarello, *J. Catal.* **2019**, *375*, 135.
- [18] T. Liang, A. C. Antony, S. A. Akhade, M. J. Janik, S. B. Sinnott, *J. Phys. Chem. A* **2018**, *122*, 631.
- [19] M. Otani, I. Hamada, O. Sugino, Y. Morikawa, Y. Okamoto, T. Ikeshoji, *Phys. Chem. Chem. Phys.* **2008**, *10*, 3609.
- [20] C. D. Taylor, S. A. Wasileski, J.-S. Filhol, M. Neurock, *Phys. Rev. B* **2006**, *73*, 165402.
- [21] N. Bonnet, N. Marzari, *Phys. Rev. Lett.* **2013**, *110*, 086104.
- [22] S. Sakong, M. Naderian, K. Mathew, R. G. Hennig, A. Groß, *J. Chem. Phys.* **2015**, *142*, 234107.
- [23] V. Tripkovic, M. E. Björketun, E. Skúlason, J. Rossmeisl, *Phys. Rev. B* **2011**, *84*, 115452.
- [24] E. Skúlason, G. S. Karlberg, J. Rossmeisl, T. Bligaard, J. Greeley, H. Jónsson, J. K. Nørskov, *Phys. Chem. Chem. Phys.* **2007**, *9*, 3241.
- [25] S. Schnur, A. Groß, *New J. Phys.* **2009**, *11*, 125003.
- [26] S. Nie, P. J. Feibelman, N. C. Bartelt, K. Thürmer, *Phys. Rev. Lett.* **2010**, *105*, 026102.
- [27] P. J. Feibelman, N. C. Bartelt, S. Nie, K. Thürmer, *J. Chem. Phys.* **2010**, *133*, 154703.
- [28] M. H. Hansen, C. Jin, K. S. Thygesen, J. Rossmeisl, *J. Phys. Chem. C* **2016**, *120*, 13485.
- [29] L. Bellarosa, R. García-Muelas, G. Revilla-López, N. López, *ACS Cent. Sci.* **2016**, *2*, 109.
- [30] H. H. Kristoffersen, T. Vegge, H. A. Hansen, *Chem. Sci.* **2018**, *9*, 6912.
- [31] R. Kronberg, K. Laasonen, *J. Phys. Chem. C* **2020**, *124*, 13706.
- [32] T. Roman, A. Groß, *Catal. Today* **2013**, *202*, 183.
- [33] S. Sakong, A. Groß, *J. Chem. Phys.* **2018**, *149*, 084705.

- [34] A. C. T. van Duin, S. Dasgupta, F. Lorant, W. A. Goddard III, *J. Phys. Chem. A* **2001**, *105*, 9396.
- [35] K. Chenoweth, A. C. T. van Duin, W. A. Goddard, *J. Phys. Chem. A* **2008**, *112*, 1040.
- [36] W. J. Mortier, S. K. Ghosh, S. Shankar, *J. Am. Chem. Soc.* **1986**, *108*, 4315.
- [37] D. Fantauzzi, J. Bandlow, L. Sabo, J. E. Mueller, A. C. T. van Duin, T. Jacob, *Phys. Chem. Chem. Phys.* **2014**, *16*, 23118.
- [38] M. V. Fedkin, Y. K. Shin, N. Dasgupta, J. Yeon, W. Zhang, D. van Duin, A. C. T. van Duin, K. Mori, A. Fujiwara, M. Machida, H. Nakamura, M. Okumura, *J. Phys. Chem. A* **2019**, *123*, 2125.
- [39] G. te Velde, F. M. Bickelhaupt, E. J. Baerends, C. Fonseca Guerra, S. J. A. van Gisbergen, J. G. Snijders, T. Ziegler, *J. Comb. Chem.* **2001**, *22*, 931.
- [40] E. J. Baerends, et al., ADF2017, SCM, Theoretical Chemistry, Vrije Universiteit, Amsterdam, The Netherlands, <https://www.scm.com>.
- [41] S. Nosé, *J. Chem. Phys.* **1984**, *81*, 511.
- [42] W. G. Hoover, *Phys. Rev. A* **1985**, *31*, 1695.
- [43] C. K. Jung, L. Braunwarth, A. Sinyavskiy, T. Jacob, Thermodynamic Description of Interfaces applying the 2PT method on ReaxFF Molecular Dynamics simulations **2021**.
- [44] L. Martínez, R. Andrade, E. G. Birgin, J. M. Martínez, *J. Comb. Chem.* **2009**, *30*, 2157.
- [45] S.-T. Lin, M. Blanco, W. A. Goddard, *J. Chem. Phys.* **2003**, *119*, 11792.
- [46] S.-T. Lin, P. K. Maiti, W. A. Goddard, *J. Phys. Chem. B* **2010**, *114*, 8191.
- [47] W. Humphrey, A. Dalke, K. Schulten, *J. Mol. Graphics* **1996**, *14*, 33.
- [48] J. A. Gauthier, C. F. Dickens, H. H. Heenen, S. Vijay, S. Ringe, K. Chan, *J. Chem. Theory Comput.* **2019**, *15*, 6895.
- [49] V. Climent, G. Attard, J. Feliu, *J. Electroanal. Chem.* **2002**, *532*, 67.
- [50] A. Frumkin, O. Petrii, *Electrochim. Acta* **1975**, *20*, 347.
- [51] N. Abidi, K. R. G. Lim, Z. W. Seh, S. N. Steinmann, *WIREs Comp. Mol. Sci.* **2020**, *n/a*, e1499.
- [52] M. Otani, O. Sugino, *Phys. Rev. B* **2006**, *73*, 115407.
- [53] A. Y. Lozovoi, A. Alavi, *Phys. Rev. B* **2003**, *68*, 245416.
- [54] J.-B. Le, J. Cheng, *Curr. Opin. Electrochem.* **2021**, *27*, 100693.
- [55] M. Wakisaka, H. Suzuki, S. Mitsui, H. Uchida, M. Watanabe, *Langmuir* **2009**, *25*, 1897.
- [56] M. Wakisaka, Y. Udagawa, H. Suzuki, H. Uchida, M. Watanabe, *Energy Environ. Sci.* **2011**, *4*, 1662.
- [57] A. M. Gómez-Marín, J. Clavilier, J. M. Feliu, *J. Electroanal. Chem.* **2013**, *688*, 360.
- [58] J. Chen, S. Luo, Y. Liu, S. Chen, *ACS Appl. Mater. Interfaces* **2016**, *8*, 20448.
- [59] J. Huang, A. Malek, J. Zhang, M. H. Eikerling, *J. Phys. Chem. C* **2016**, *120*, 13587.
- [60] T. Jacob, W. A. Goddard III, *J. Am. Chem. Soc.* **2004**, *126*, 9360.
- [61] L. D. Site, L. M. Ghiringhelli, O. Andreussi, D. Donadio, M. Parrinello, *J. Phys. Condens. Matter* **2007**, *19*, 242101.
- [62] T. Ikeshoji, M. Otani, I. Hamada, O. Sugino, Y. Morikawa, Y. Okamoto, Y. Qian, I. Yagi, *AIP Adv.* **2012**, *2*, 032182.
- [63] Z. Zeng, J. Greeley, *Nano Energy* **2016**, *29*, 369.
- [64] E. U. Franck, *Ber. Bunsen-Ges.* **1990**, *94*, 93.
- [65] D. T. Limmer, A. P. Willard, P. Madden, D. Chandler, *Proc. Nat. Acad. Sci.* **2013**, *110*, 4200.

Manuscript received: May 16, 2022

Revised manuscript received: September 19, 2022

Accepted manuscript online: September 19, 2022

Version of record online: October 26, 2022